PCCP

PAPER

View Article Online
View Journal | View Issue

Cite this: *Phys. Chem. Chem. Phys.*, 2018, **20**, 14785

Molecular mechanism of 15-lipoxygenase allosteric activation and inhibition†

Hu Meng,[a] Ziwei Dai,[b] Weilin Zhang,[b] Ying Liu[ab] and Luhua Lai*[abc]

Received 23rd December 2017,
Accepted 8th May 2018

DOI: 10.1039/c7cp08586a

rsc.li/pccp

Human reticulocyte 15-lipoxygenase (15-LOX) plays an important role in inflammation resolution and is also involved in many cancer-related processes. Both an activator and an inhibitor will serve as research tools for understanding the biological functions of 15-LOX and provide opportunities for drug discovery. In a previous study, both allosteric activators and inhibitors of 15-LOX were discovered through a virtual screening based computational approach. However, why molecules binding to the same site causes different effects remains to be disclosed. In the present study, we used previously reported activator and inhibitor molecules as probes to elucidate the mechanism of allosteric regulation of 15-LOX. We measured the influences of the allosteric activator and inhibitor on the enzymatic reaction rate and found that the activator increases 15-LOX activity by preventing substrate inhibition instead of increasing the turnover number. The inhibitor can also prevent substrate inhibition but decreases the turnover number at the same time, resulting in inhibition. Molecular dynamics simulations were conducted to help explain the underlying mechanism of allostery. Both the activator and inhibitor were demonstrated to be able to prevent 15-LOX from transforming into potentially inactive conformations. Compared to the activator, the inhibitor molecule restrains the motions of residues around the substrate binding site and reduces the flexibility of 15-LOX. These results explained the different effects between the activator and the inhibitor and shed light on how to effectively design novel activator molecules.

Introduction

Human reticulocyte 15-lipoxygenase (15-LOX) is a 75 kDa fatty acid dioxygenase. It inserts molecular oxygen and abstracts hydrogen in a stereoselective reaction with 1,4-*cis*-pentadiene units present in polyunsaturated fatty acids such as arachidonic acid (AA) and linoleic acid (LA) and creates 15-hydroxyecosatetraenoic acid (15-HETE) and 13-hydroxyoctadecadienoic acid (13-HODE), respectively.[1] Its product, 15-HETE, can be further converted into lipoxins, which possess anti-inflammatory activity as well as inflammation resolution capacity.[2,3] For these reasons, development of 15-LOX activators may lead to the discovery of a new generation of anti-inflammatory drugs. It was recently reported that 15-LOX is also involved in many cancer-related processes and may act as a carcinogen or a tumor suppressor.[4] The dichotomy in 15-LOX actions complicates the study of this enzyme, and future research is needed to elucidate its role in cell signaling.

Compared to designing conventional active-site competitors for specific protein targets, allosteric effectors can both increase or decrease the activity of the target, which is difficult to achieve with orthosteric drugs.[5] Therefore, developing allosteric effectors, especially activators, will provide new research tools for understanding the function of 15-LOX and new opportunities for drug discovery. In a previous study, we have proposed a rational strategy for allosteric site identification and binding molecule design.[6] Both activator and inhibitor molecules were discovered for the newly identified allosteric site in 15-LOX (Fig. 1). The activator, PKUMDL_MH_1001 (compound **1**), increased the activity of human reticulocyte 15-LOX both *in vitro* and *ex vivo*. The binding site of compound **1** was confirmed by mutations at the predicted allosteric site. A recent study[7] shows that compound **1** could activate cellular lipoxygenase and enhance ferroptotic cell death in certain tumor cell lines. However, why molecules binding to the same site cause different effects (either activation or inhibition) remains to be disclosed. In the present study, we tried to elucidate the mechanism of allosteric regulation of 15-LOX using combined enzyme catalysis experimental study and molecular dynamics (MD) simulations. The influences of an allosteric activator and inhibitor on 15-LOX conformation, flexibility, and collective motions were analyzed. A model of 15-LOX allostery was proposed which may aid in the design of new activators or inhibitors.

[a] *BNLMS, State Key Laboratory for Structural Chemistry of Unstable and Stable Species, College of Chemistry and Molecular Engineering, Peking University, A518 Chemistry Building, 202 Chengfu Road, Beijing 100871, China. E-mail: lhlai@pku.edu.cn; Fax: +86-10-62751725; Tel: +86-10-62757486*
[b] *Center for Quantitative Biology, Peking University, A518 Chemistry Building, 202 Chengfu Road, Beijing 100871, China*
[c] *Peking-Tsinghua Center for Life Sciences, Peking University, A518 Chemistry Building, 202 Chengfu Road, Beijing 100871, China*

† Electronic supplementary information (ESI) available. See DOI: 10.1039/c7cp08586a

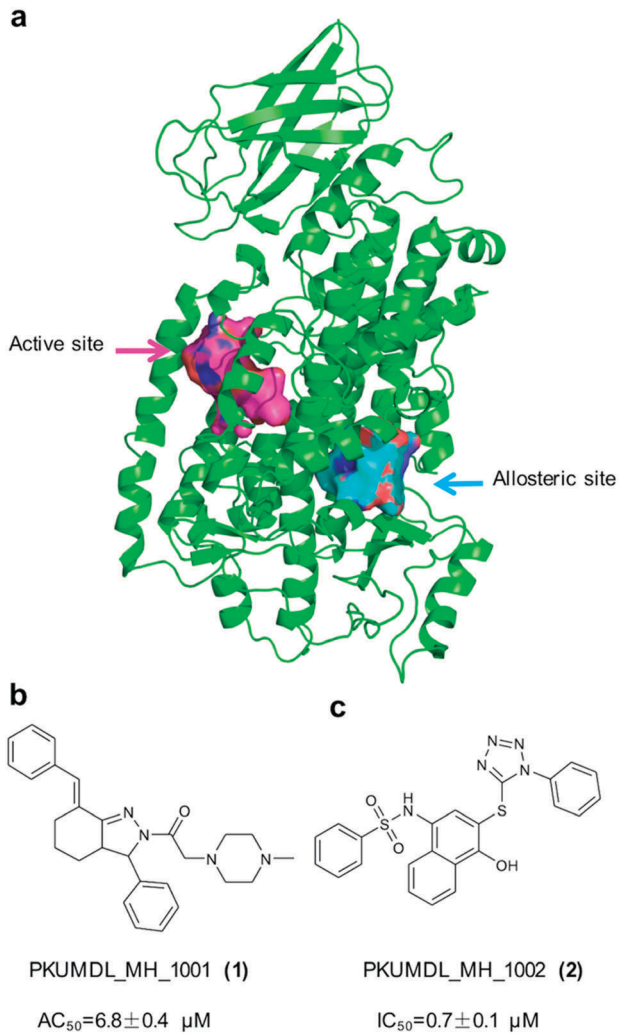

Fig. 1 Allosteric site and allosteric effectors of 15-LOX. (a) Location of the active site and allosteric site identified by a computational approach involving protein correlated motion analysis and surface cavity druggability analysis. (b) Chemical structure of the allosteric activator, PKUMDL_MH_1001 (**1**). (c) Chemical structures of the allosteric inhibitor, PKUMDL_MH_1002 (**2**). The half maximal activation concentration (AC_{50}) and the half maximal inhibitory concentration (IC_{50}) are listed under (b) and (c), respectively.

Materials and methods

Chemicals and reagents

AA was purchased from Cayman Chemical (Ann Arbor, MI, USA). Compound **1** ((*E*)-1-(7-benzylidene-3-phenyl-3,3*a*,4,5,6,7-hexahydroindazol2-yl)-2-(4-methylpiperazin-1-yl)ethanone, SPECS ID: AO-476/43305824) and compound **2** (*N*-{4-hydroxy-3-[(1-phenyl-1*H*-tetraazol-5-yl)sulfanyl]-1-naphthyl}benzenesulfonamide, AQ-390/43238223) were purchased from SPECS. NMR or LC-MS data for these compounds were available through the website. The purities of the compounds exceed 95% which was confirmed by LC-MS data available through the SPCES website. Compound **1** was not in the pan-assay interference compounds (PAINS) list. Compound **2** was in the list belonging to the category of "redox activity". Therefore, we tested the stability of compound **2** by LC-MS. The peak area of compound **2** after *in vitro* assay was 100 ± 1% of that measured before reaction (normalized by volume). Full concentration response curves, and binding constant data for compound **1** and compound **2** are listed in the ESI.† Ampicillin, clarithromycin, isopropyl β-thiogalactoside, dithiothreitol, ethylenediaminetetraacetic acid, phenylmethanesulfonyl fluoride, and dimethyl sulfoxide (DMSO) were obtained from Amresco (Solon, OH, USA). Water was purified with a Milli-Q Reagent Water System (Millipore, Billerica, USA).

Enzyme kinetics assay of 15-LOX

Molecular cloning, protein expression, and purification of 15-LOX were carried out as described previously[6] and details can be found in the ESI.† Briefly, wild-type human 15-LOX was amplified from a cDNA clone (UniProtKB: P16050, MGC:34638 IMAGE:5179700; Source BioScience). The amplified fragments of 15-LOX were ligated into the pET-28a vector resulting a plasmid, pET-15LOX-h28, encoding the 15-LOX protein with an N-terminal His6 tag. This plasmid was transferred into *E. coli* strain Rosetta <DE3> for expression of His6-tagged 15-LOX. A nickel-nitrilotriacetic acid column (HisTrap HP; GE Healthcare) and an anion-exchange column (Q Trap HP; GE Healthcare) were used for protein purification. The purities of the protein samples (>95%) were confirmed by SDS/PAGE on a polyacrylamide gel (10%, w/v) with a mini-vertical gel system (Bio-Rad). The enzyme reaction rates were assessed by measuring the formation of product at 235 nm (ε = 25 000 M^{-1} cm^{-1}).[8] The enzyme was added to quartz 96-well microtiter plates in sodium phosphate buffer (100 mM, pH 7.4) and incubated with a compound (dissolved in DMSO) at room temperature for one minute. Reactions were initiated by adding the substrate (AA) at different concentrations. The absorbance of 15-HpETE was monitored on a plate reader (Synergy, Biotek).

Parameter estimation and simulation of the model

We applied nonlinear least squares fitting to evaluate kinetic parameters in the model. 56 rates of reaction measured under different combinations of concentrations for the allosteric regulators and the substrate, arachidonic acid, were used in the fitting. The cost function minimized in the fitting, $C(\theta)$, was defined in a weighted sum of squares form in which the residues were normalized in a χ^2-criterion, plus a penalty term to confine the parameters K_a, K_m, K_i and K_{cat}/K_m:

$$C(\theta) = \chi^2(\theta) + P(\theta)$$

$$\chi^2(\theta) = \sum_{i=1}^{n} \left(\frac{v_i(\theta) - v_{it}}{\sigma_i} \right)^2$$

$$P(\theta) = 100 \times \left[D\left(\log_{10} \frac{K_{off,Inh}}{K_{on,Inh}}, -4, 2 \right) + D\left(\log_{10} \frac{K_{off,Act}}{K_{on,Act}}, -4, 2 \right) + D\left(\log_{10} \frac{K_{off,S}}{K_{on,S}}, -4, 2 \right) + D\left(\log_{10} \frac{K_{off}}{K_{on}}, -3, 1 \right) + D\left(\log_{10} \frac{K_{cat} K_{on}}{K_{off}}, -\infty, 4 \right) \right]$$

$$D(a,b,c) = \begin{cases} (b-a)^2, & \text{if } a < b \\ 0, & \text{if } b \le a \le c \\ (a-c)^2, & \text{if } a > c \end{cases}$$

In which θ is the parameter vector, $v_i(\theta)$ is the ith reaction rate simulated by the model under parameter vector θ, v_{it} is the 'true' reaction rate measured experimentally, n is the number of data points and σ_i is the standard deviation of v_{it}. The cost function is minimized using differential simulated annealing from 10 different initial guesses to avoid local minima.[9] Ordinary differential equations were solved using the solver suitable for stiff systems, gsl_odeiv2_step_msbdf, in the GNU Scientific Library.[10] Reaction rates were approximated by the average amount of the product 15-HPETE formed per second in the first 20 seconds of simulation.

Bayesian credible intervals of the parameters were evaluated by Markov chain Monte Carlo (MCMC) sampling using the Metropolis algorithm. Using the uniform prior distribution, the posterior distribution of parameter vector θ, which is sampled by the MCMC, is defined as:

$$\pi(\theta|v) = \frac{L(\theta, v)}{\int L(\theta, v)\mathrm{d}\theta}$$

In which $L(\theta,v)$ is the likelihood under the assumption that all noises are Gaussian-distributed:

$$L(\theta, v) = \frac{1}{(2\pi)^{\frac{n}{2}} \prod_{i=1}^{n} \sigma_i} \mathrm{e}^{-\frac{1}{2}\chi^2(\theta)}$$

The length of the Markov chain was set to 100 000. After discarding all parameter vectors with the parameters K_a, K_m, K_i and K_{cat}/K_m falling out of the region defined previously, the remaining parameter vectors were sorted by their corresponding $\chi^2(\theta)$, then parameter vectors with the smallest 95% $\chi^2(\theta)$ were kept to evaluate the credible intervals for each parameter.

Comparative modeling

We used the PRIME (Schrödinger, LLC) comparative modeling environment to construct a model of human 15-lipoxygenase from rabbit 15*S*-lipoxygenase (PDB code: 2P0M, 81% sequence identity, similarity: 90%). We retained the metal iron and the geometries of the conserved side chains. In addition, we optimized and minimized the side chains of non-conserved residues.

Molecular dynamics simulations

We performed molecular dynamics simulations in explicit solvent with the Desmond[11] software package and OPLS-AA/SPC force field.[12] The protein was placed in an orthorhombic simulation with a buffer of 10 Å on each side. Na^+ and Cl^- ions were added to neutralize the system, and then 0.05 M NaCl was added. Minimization was initially performed with the solute positions restrained at 50 kcal mol^{-1} $Å^{-1}$ for 2000 steps. The solute positions were unrestrained, and minimization proceeded for another 2000 steps. Next, heavy atoms in the solute were restrained at 50 kcal mol^{-1} $Å^{-1}$. *NVT* molecular dynamic simulations were performed at 10 K for 12 picoseconds (ps). This was followed by *NPT* equilibration at 10 K for 12 ps. Then, the system was simulated for another 34 ps at 300 K with the same settings. Finally, restraints on heavy atoms were removed, and the system was simulated for an additional 24 ps at 300 K with a thermostat-relaxation rate of 0.1 ps^{-1} and barostat-relaxation rate of 2 ps^{-1}.

After minimization and equilibration, multiple (different random seed) production runs of 10 ns were performed on each system with the Martyna–Tobias–Klein integrator[13] at 300 K and 1 atm. Snapshots were taken every 1.0 ps. Production runs were collected as follows. We simulated 15-LOX under three different starting conditions: (i) apo structure; (ii) structure in complex with the activator **1**; and (iii) complex with the allosteric inhibitor, **2**. Six production runs of 100 ns were performed for each system. The small molecules were docked into the allosteric site as described previously.[6] The detailed procedure is described in the ESI.†

Clustering conformations

Six production simulations of each of the three different starting conditions were combined to three new trajectories for clustering purposes, and clustering was performed in Gromacs with QT clustering ("cluster-method gromos")[14] and a cutoff of 0.2 nm. Snapshots were taken every 10 ps. Representative conformations (middle conformation in the cluster which was larger than 10%) from the last 10 ns in the trajectories were inspected. All representative conformations were analyzed by the program CAVITY[15,16] using the default parameters. The volume of cavities in each conformation was given by CAVITY. The volume of cavities was detected by eraser ball with a radius length of 10.0 Å. Solvent radius was 1.5 Å. The starting conformation and one representative conformation of apo 15-LOX were analyzed using SiteMap[17] (Schrödinger, LLC) with default parameters to confirm the results from CAVITY.

Root mean square fluctuation of the conformations

Six production simulations of each of the three different starting conditions were combined into three new trajectories for RMS fluctuation. RMS fluctuation was calculated in Gromacs using default parameters.

Principal component analysis on the models of 15-LOX

Eighteen 100 ns length MD simulations were performed on the model of 15-LOX. We simulated 15-LOX under three different starting conditions: (i) apo structure, (ii) structure in complex with the activator (**1**), and (iii) structure in complex with an allosteric inhibitor (**2**) (six production runs of 100 ns were performed for each starting structure). All production simulations were combined for PCA analysis. The covariance matrix was calculated and diagonalized in Gromacs (gmx covar). The eigenvectors are written to a trajectory file. The eigenvectors were analyzed with Gromacs program, gmx anaeig. The first principal component (PC1) captures 46% of the structural variances, the second principal component (PC2) accounts for 34%.

Docking of arachidonic acid to the active site of the apo conformation

Molecular docking was conducted using AutoDock Vina.[18] The AA was docked into the active site of the apo 15-LOX conformation using the following parameters: number of modes, 8;

exhaustiveness, 8; energy range, 3. We docked AA into two different grid boxes. The size of the grid boxes was 22 × 22 × 22 Å. The center of grid boxes was at the center of residues: 166, 170, 174, 394, 395, 600, 604–609, 657–659, 601 and the center of residues: 144, 166, 171, 174, 175, 361, 365, 366, 399, 400, 402–404, 407, 408, 596, 601.

Community network analysis

We used a method previously introduced by Luthey-Schulten and coworkers.[19] Briefly, our MD simulation trajectories were combined by apo 15-LOX, 15-LOX with activator, or 15-LOX with inhibitor. Combined trajectories were used to conduct a network analysis which uses local coupled motions between pairs of residues to track allosteric signaling. We assigned one node to each amino acid in 15-LOX. Amino acid nodes were centered Cα atoms. We incorporate dynamics into our definition and draw edges between nodes whose residues are within a cutoff distance (7.0 Å) for at least 75% of an MD trajectory. The cross-correlations calculated from atomic fluctuations were used to weight each edge. The time averaged connectivity of the nodes was used to identify the substructure or communities in the network. The optimal community distribution was calculated using the Girvan–Newman algorithm.[20]

Protein–ligand contacts analysis

The last eight nanoseconds of the MD trajectories were analyzed by using the Simulation Interaction Diagrams module in Desmond (Schrödinger, LLC) using default parameters. Protein interactions with the ligand were monitored throughout the simulation. Protein–ligand interactions (or 'contacts') were categorized into four types: hydrogen bonds, hydrophobic, ionic and water bridges. Hydrogen bonds between a protein and a ligand can be further broken down into four subtypes: backbone acceptor; backbone donor; side-chain acceptor; side-chain donor. The geometric criteria for a protein–ligand H-bond are: distance of 2.5 Å between the donor and acceptor atoms (D–H···A); a donor angle of 120° between the donor–hydrogen–acceptor atoms (D–H···A); and an acceptor angle of 90° between the hydrogen-acceptor-bonded atoms (H···A–X). Hydrophobic contacts fall into three subtypes: pi–cation; pi–pi; and other, non-specific interactions. The geometric criteria for hydrophobic interactions are as follows: pi–cation—aromatic and charged groups within 4.5 Å; pi–pi—two aromatic groups stacked face-to-face or face-to-edge; other—a non-specific hydrophobic sidechain within 3.6 Å of a ligand's aromatic or aliphatic carbons. Ionic interactions or polar interactions, are between two oppositely charged atoms that are within 3.7 Å of each other and do not involve a hydrogen bond. All ionic interactions are broken down into two subtypes: those mediated by a protein backbone or side chains. Water bridges are hydrogen-bonded protein–ligand interactions mediated by a water molecule. The hydrogen-bond geometry is slightly relaxed from the standard H-bond definition. The geometric criteria for a protein–water or water–ligand H-bond are: a distance of 2.7 Å between the donor and acceptor atoms (D–H···A); a donor angle of 110° between the donor–hydrogen–acceptor atoms (D–H···A); and an acceptor angle of 80° between the hydrogen–acceptor-bonded atoms (H···A–X). The stacked bar charts were normalized over the course of the trajectory: for example, a value of 0.7 suggests that 70% of the simulation time the specific interaction is maintained. Values over 1.0 are possible as some protein residue may make multiple contacts of the same subtype with the ligand. Hydrogen bonds: (H-bonds) play a significant role in ligand binding.

Results

Enzyme kinetics assays

It was reported that the activity of 15-LOX can be inhibited by its own substrate at high concentration.[21] Thus, the substrate, AA, also acts as an allosteric inhibitor at high concentration. To unravel the complex interactions between 15-LOX, substrate, and exogenous allosteric effectors, firstly, we measured the enzymatic reaction velocity of recombinant human reticulocyte 15-LOX at different concentrations of substrate (AA) without any exogenous allosteric compounds *in vitro*. Along with the increase of AA concentration, the reaction rate initially increased but then dramatically decreased, similar to a previous report[21] (Fig. 2a, red dots). The maximal reaction velocity was observed when the concentration of AA was 39 μM which was lower than the critical micellar concentration (73 μM).[22] This implied that the substrate inhibition was caused by allosteric binding of a second molecular AA instead of physical effects triggered by formation of lipid micelles. In the presence of the activator, compound **1**, substrate inhibition was gradually released along with the increase of the activator concentration (Fig. 2a). The results of kinetic assays suggested that our activator preserves 15-LOX activity at high substrate concentrations by protecting the enzyme from inhibition by the second molecule of AA. We also tested the dose-dependent effect of the allosteric inhibitor, compound **2** (Fig. 2b). The presence of compound **2** decreased the reaction rate significantly even at low AA concentration before AA inhibition occurred, demonstrating that this compound should occupy a site other than that the second AA binding site.

Model for the 15-LOX enzyme reaction with allosteric regulation

The experimental data cannot be fitted by a Lineweaver–Burk plot due to the substrate inhibition effect. Therefore, to understand the allosteric mechanism quantitatively, we proposed a reaction model (Fig. 2c), which includes the following steps: (1) 15-LOX has two AA binding sites, the strong one is the active site and the weak one is the substrate inhibition site. (2) 15-LOX binds to compound **1** or **2** using an allosteric site other than the two AA binding sites. (3) 15-LOX converts AA into a product with different k_{cat} values depending on whether 15-LOX is bound to a single substrate, an allosteric effector plus substrate, two substrate molecules, or an allosteric effector plus two substrate molecules. Following this model, the kinetic parameters were derived by fitting the experimental data of reaction rates *versus* substrate concentrations under different conditions

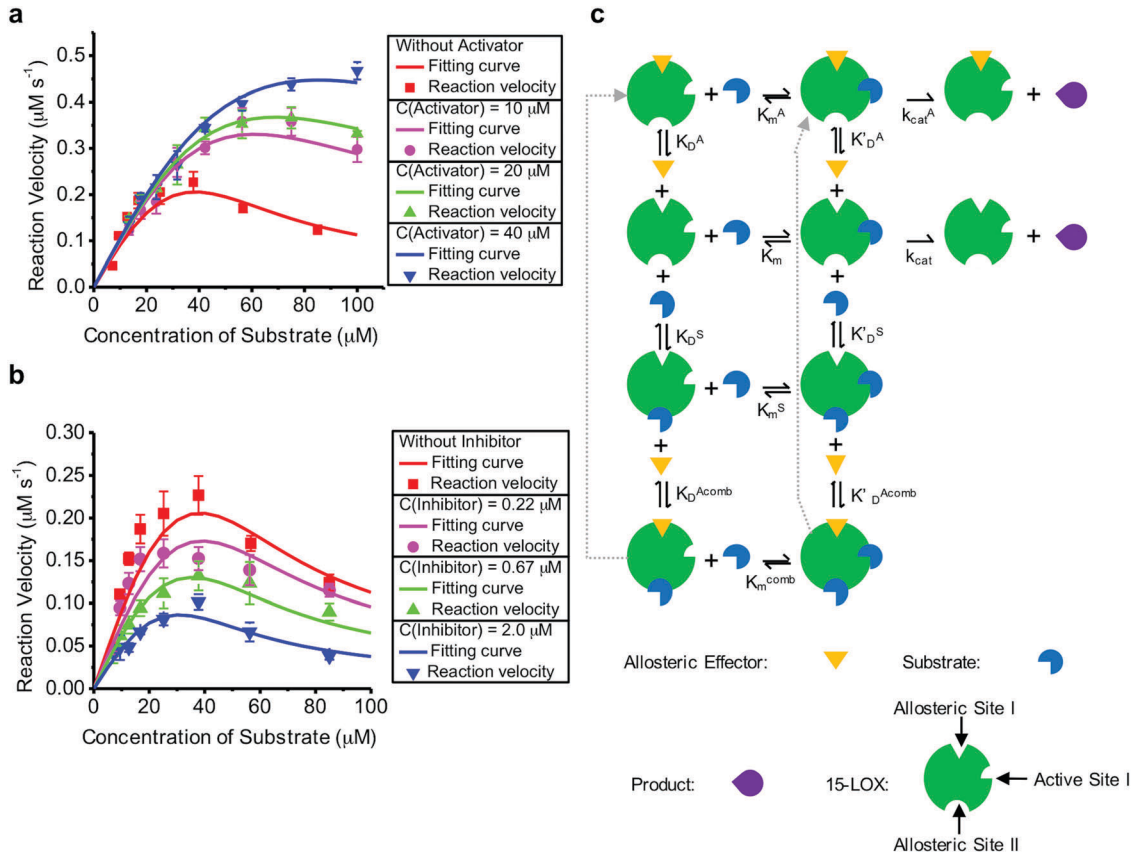

Fig. 2 Substrate inhibition curve of 15-LOX and influence of allosteric effectors on the enzyme kinetics. (a) Reaction velocity *vs.* AA concentration curve when different concentrations of activator, compound **1** were present. (b) Reaction velocity *vs.* AA concentration curve when different concentrations of inhibitor, compound **2** were present. Data shown represent the mean ± SEM (n = 3). (c) Scheme of substrate inhibition mechanism. This scheme is simplified by eliminating species with low concentration and reaction steps which rarely occur. The full version for the reaction mechanism scheme is in Fig. S1 (ESI†).

(curves in Fig. 2a, more detailed kinetic parameters given by fitting are shown in Table S1, ESI†).

For wild-type 15-LOX, the optimal value of catalytic constant k_{cat} given by fitting was 1.00×10^3 s^{-1} (95% credible interval: 93.3 s^{-1} to 1.00×10^3 s^{-1}), which was drastically reduced to a negligible k_{cat}^{S} of 7.82×10^{-11} s^{-1} (95% credible interval: 9.40×10^{-12} s^{-1} to 2.70×10^{-9} s^{-1}) for the substrate inhibition state. The binding strength of the second AA was deteriorated after either allosteric activator or inhibitor binding, with a dissociation constant K_D^S of 5.02 mM (95% credible interval: 5.02 mM to 11.9 mM) increased to K_D^{Scomb} of 8.92×10^2 mM (95% credible interval: 31.8 mM to 4.63×10^3 mM) or 1.74×10^4 mM (95% credible interval: 1.47×10^4 mM to 9.01×10^6 mM). At the same time, the binding affinity of an allosteric activator or inhibitor increased after the binding of the second AA (values of K_D^{Acomb} became three magnitudes smaller than K_D^A, Table S1, ESI†). This indicated that both the allosteric activator and inhibitor molecule can prevent the enzyme binding to the second AA molecule by allosteric effects (binding to a different site). The calculated k_{cat} (k_{cat}^A) of the activator bound enzyme was in a similar range (95% credible interval: 82.4 s^{-1} to 3.01×10^2 s^{-1}) as the regulator-free enzyme (95% credible interval: 93.3 s^{-1} to 1.00×10^3 s^{-1}). Although the activator actually decreased the k_{cat} a little bit, it drastically reduced the binding affinity of the second AA, thus increasing enzyme activity at a high concentration of AA. In contrast, the allosteric inhibitor, **2**, decreased k_{cat} significantly regardless of whether 15-LOX bound to the second AA or not (95% credible interval: 8.3 s^{-1} to 73.3 s^{-1}). This kinetic model suggests that the allosteric activator and inhibitor alter enzymatic activity through complex mechanisms by influencing the second AA binding and enzyme catalytic rates. We noticed that the turn over number given by our model was much larger than previously reported values.[23] However, because of the existence of substrate inhibition, the apparent turn over number should be much lower.

Conformational changes of 15-LOX

To reveal the mechanism of 15-LOX allosteric activation and inhibition, we performed a series of molecular dynamics simulations and analyzed conformational changes induced by the allosteric effector binding. We simulated 15-LOX under three different starting conditions: (i) apo structure; (ii) structure in complex with the activator, compound **1**; and (iii) complex with the allosteric inhibitor, compound **2**. Snapshots (every 10 ps) of MD simulations in the last 10 ns were clustered with a cutoff of 0.2 nm. The central conformations of large clusters (>10% in combined trajectory)

were chosen as representative conformations. All representative conformations were analyzed using the CAVITY[15,16] program to detect the cavities in the protein. SiteMap[17] (Schrödinger, LLC) was also used, which gave the same list of potential binding sites (Table S2, ESI†). The results are listed in Table 1. Representative conformations are shown in Fig. 3 and Fig. S2 (ESI†).

The substrate binding pockets of apo 15-LOX in the last 10 ns in all six trajectories (Table 1) were open to the protein surface (Fig. 3 and Fig. S2, ESI†). This kind of conformation may facilitate substrate binding. In three (representative conformation of cluster 1, 2, and 4) out of the four representative conformations, the substrate-binding pocket is connected to another cavity between the N-terminal domain and catalytic domain leaving two entrances on the surface of the protein (Fig. 3b and Fig. S2, ESI†). The volume of these pockets is almost twice as large as that in the starting conformation (Table 1). Molecular docking was conducted using AutoDock Vina.[18] We found that the pocket in the representative conformation of cluster 1 could bind two molecules of substrates simultaneously (Fig. 3b). One substrate binds at the active site (with a docking score of -7.1 kcal mol^{-1}) and another at a position away from the catalytic center (with a docking score of -6.6 kcal mol^{-1}). The binding of the second AA molecule may affect the catalytic reaction and cause the substrate inhibition phenomenon we observed in experimental studies. This assumption is supported by previous studies[24,25] on rabbit 15-LOX, reporting that a few residues near the substrate binding site might be in contact with excessive amounts of substrate fatty acid and endogenous allosteric ligand to cause inhibition.

After binding the activator, the entrance of the substrate binding site was open similar to that in the starting conformation (Fig. S2f–j, ESI†). In two (representative conformation of clusters 5 and 9) out of the five representative conformations, the volume of the catalytic center increased as that in apo 15-LOX did (Table 1). When 15-LOX binds the activator, none of these substrate binding sites connect to the cavity between the N-terminal domain and catalytic domain (Fig. S2f–j, ESI†). These results indicate that the allosteric activator stabilized the right conformations of the enzyme and preserved 15-LOX activity by protecting the enzyme from inactive conformations induced or stablized by an excessive amount of AA. The allosteric inhibitor, compound **2**, induced similar conformational changes of 15-LOX as the activator did. None of the substrate binding sites in the conformations of the inhibitor binding 15-LOX formed the second entrance between the N-terminal domain and catalytic domain. (Fig. S2k–o, ESI†). These results explain why both an allosteric activator and inhibitor can decrease the binding affinity of the second molecule of AA to 15-LOX.

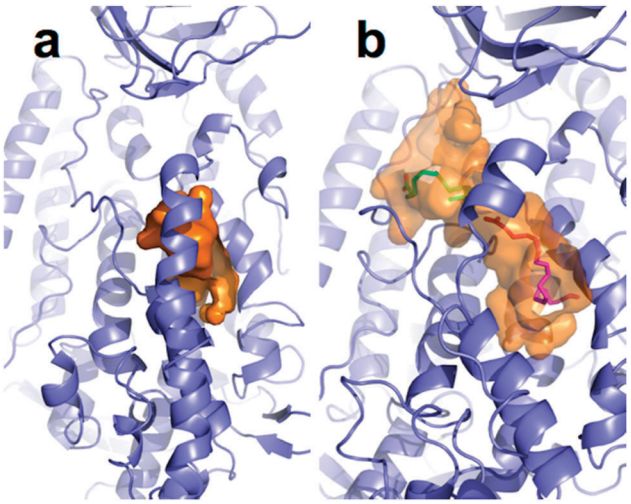

Fig. 3 Conformational changes of 15-LOX at the active site in molecular dynamics simulations. (a) The surfaces of cavities at the active site in the starting conformation of apo 15-LOX and (b) representative conformation of apo 15-LOX in the last 10 ns of MD simulations are shown in this figure. Two molecules of AA were docked in apo 15-LOX. One was at the active site (magenta) and another one was at a position away from the catalytic center (green). Figures of other major conformations are in the ESI.†

Allosteric effectors change the flexibility of 15-LOX differently

The activator, compound **1**, and inhibitor, compound **2**, induced similar conformational changes in MD simulations. To determine

Table 1 The active site volume in representative conformations of 15-LOX in each trajectory of the last 10 ns MD simulations

Starting conditions of MD simulation	Clusters	Relative cluster size (% in all six MD runs)	Volume of cavity at active site (Å^3)	Number of entrance of active site
Starting conformation	—	—	885	1
Apo 15-LOX	1	26.4	1489	2
	2	25.4	2100	2
	3	15.9	774	1
	4	14.3	2304	2
15-LOX with activator	5	27.2	1169	1
	6	10.1	741	1
	7	16.0	815	1
	8	15.9	459	1
	9	10.7	1488	1
15-LOX with inhibitor	10	10.1	480	1
	11	17.3	888	1
	12	29.4	675	1
	13	14.5	1019	1
	14	10.9	1130	1

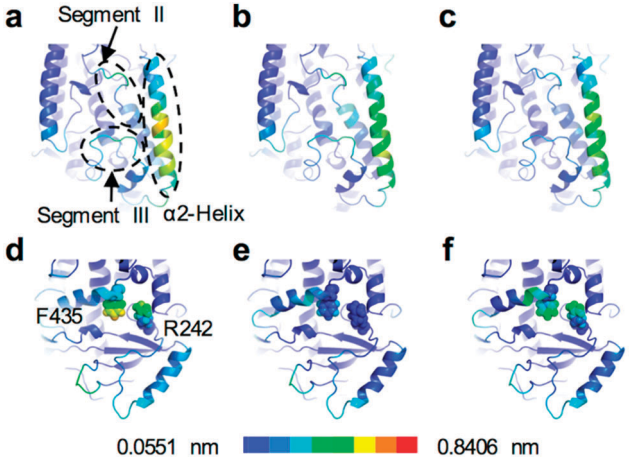

Fig. 4 RMS fluctuations of 15-LOX with and without allosteric effector in MD simulations. RMS fluctuations of (a) apo 15-LOX, (b) 15-LOX with activator, and (c) 15-LOX with inhibitor in MD simulations were calculated. RMS fluctuations of an allosteric site of (d) apo 15-LOX, (e) 15-LOX with activator, and (f) 15-LOX with inhibitor are also shown in this figure. Residues with higher values of RMSF are shown in warmer colors.

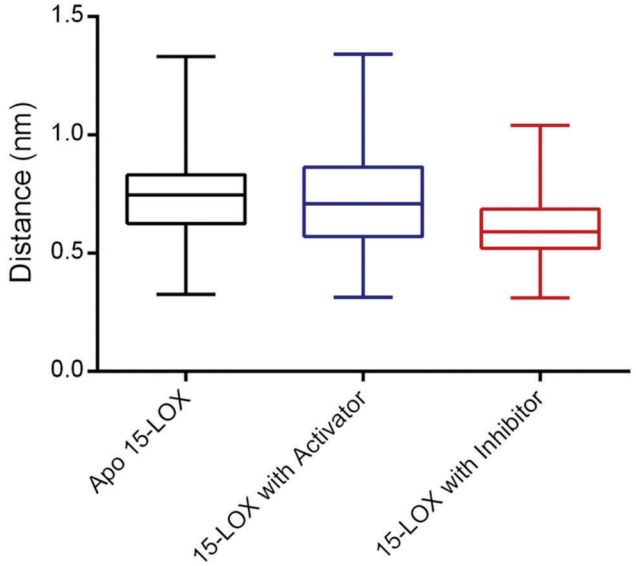

Fig. 5 The distance between the mainchain of P601 and mainchain of α2-helix. The distance between the mainchain of P601 and mainchain of α2-helix in each snapshot was calculated (N = 60 000 for each complex). The box-plot shows the median and interquartile range of the distance. Error bars indicate the extreme values.

the difference between these two types of allosteric effector, we further looked into the changes in flexibility of 15-LOX caused by these compounds. The root mean square fluctuation (RMSF) for all atoms in apo 15-LOX, 15-LOX with activator, and 15-LOX with inhibitor were calculated and shown in Fig. 4. The helix-α2 of apo 15-LOX was very variable (Fig. 4a and d). In our previous study,[6] we found that the torsion angles of R242 and F435 at the allosteric site were highly correlated with that of residues on helix-α2 and around the active site. MD simulation revealed that the allosteric site was stablized by the activator, **1**. The flexibility of helix-α2 was also decreased (Fig. 4b and e). The allosteric inhibitor, **2**, also decreased the flexibility of R242 and F435, but not as effectively as compound **1** did. The flexibility of helix-α2 was also decreased (Fig. 4c and f). Different from the activator, the inhibitor also stabilized the movement of segment II and segment III. Segment II comprising thirteen residues contains the C-terminal end of helix-α18 and the following chain of six residues. Helix-α18 is critical in shaping the substrate-binding cavity. Binding with the allosteric inhibitor restrained the movement of the loop in segment II, making the maximum and average distance between the mainchain of this loop and mainchain of α2-helix significantly smaller than that in apo 15-LOX and 15-LOX with activator (Fig. 5, the distance is defined as the minimal distant between the mainchain of P601 and the mainchain of E168-L192). These results implied that the inhibitor may hinder the conformational changes of 15-LOX at the active site and caused inhibition.

Principal component analysis of 15-LOX dynamics

To examine how allosteric effectors change the collective motions of 15-LOX, we analyzed MD trajectories using principal component analysis (PCA). All production simulations were combined for PCA analysis and projected onto the first two PCA eigenvectors. Distributions of projection along the first two eigenvectors were plotted (Fig. 6a–c). To see what types of motion the individual eigenvectors corresponded to, we filtered the original trajectory and projected out the part along the first two eigenvectors. Extreme projections along the trajectory on the first principal component (PC1) and secondary principal component (PC2) are shown in Fig. 6. The eigenvector of PC1 corresponded to the relative motion of the two domains (Fig. 6d) and twist of helix-α8 (Fig. 6f). The eigenvector of PC2 generally corresponded to the motion of helix-α2: as helix-α2 moves towards helix-α9, the corresponding PC2 value increased (Fig. 6e). The eigenvector of PC2 also involved the motions of segment II and stretch of helix-α8 (Fig. 6g). In the trajectories of apo 15-LOX, the protein can move in both the positive and negative direction around the starting conformation (PC1: −5.4, PC2: −2.6) along PC1 and PC2. The change of conformational distribution reveals that the binding of the activator stabilized the starting conformation along PC1, but induced motions in the positive direction along PC2 (Fig. 6a–c). These results implied that binding of the activator prevented helix-α2 from moving away from α9 and enable helix-α2 to move closer to α9, which may facilitate the transformation between ligand-free and ligand-bound conformations. Structures in trajectories of 15-LOX binding with inhibitor were mainly distributed on the positive side of PC1, which were obviously different from those in trajectories of apo 15-LOX and the complex with activator (Fig. 6a–c). After binding to the allosteric inhibitor, the relative motion of the two domains changed direction and the N-terminal domain moved to come in contact with the catalytic domain, which may bring 15-LOX into an inactivated state.

Community network analysis

Community network analysis can give insight into how allosteric effectors change the dynamical network of interactions within

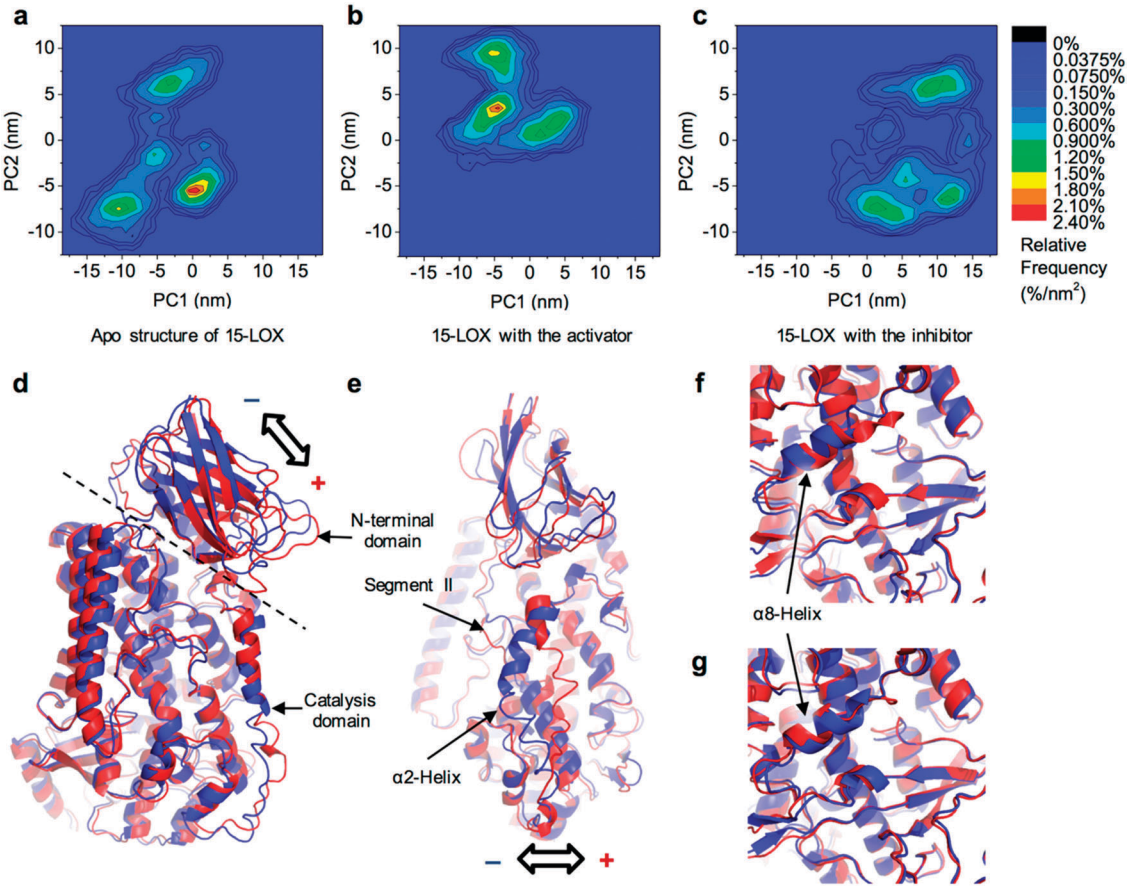

Fig. 6 Principal component analysis of 15-LOX dynamics. Two-dimensional projection graphs of (a) apo structure, (b) the 15-LOX with the activator, and (c) 15-LOX with the inhibitor on the first two PCA eigenvectors were plotted. In this graph, different colors represent different relative frequency of snapshots (every 20 ps) from the simulations. Extreme projections along the trajectory on (d and f) PC1 and (e and g) PC2 were also demonstrated. Red structures corresponded to positive extreme values of eigenvectors. Blue structures corresponded to negative extreme values of eigenvectors. Larger images of allosteric site were graphed in (f and g).

15-LOX. We used the method introduced by Luthey-Schulten and coworkers to do community network analysis.[19] Our MD simulation trajectories were used to conduct a network analysis which uses local coupled motions between pairs of residues to track allosteric signaling. In these networks, a node represented an amino acid residue. The cross-correlations calculated from atomic fluctuations were used to weight each edge. The time averaged connectivity of the nodes was used to identify the substructure or communities in the network. The optimal community distribution was calculated using the Girvan–Newman algorithm.[20] The network of Apo 15-LOX was divided into 15 communities (Fig. 7 and Table S3, ESI†). The N-terminal domain was split into community C1 and C13. The residues of the active site were separated into community C3, C7, C10, C12, and C14. The second AA binding site laid between community C1, C3, C7, and C9. Allosteric effectors bound between community C6, C12 and C15 (Fig. 7c). All three important cavities were located between multiple communities. This is reasonable because it allows the cavities to have flexibility to bind the ligand. Community C9 had weak or no connections to C1, C3, and C7 in apo 15-LOX which may explain the formation of the second AA binding site in these trajectories.

After binding an allosteric activator, the number of communities changed to 14 (Fig. 7d). We kept using the same community identity number as that in apo 15-LOX when they laid roughly in the same location but the residues may not be exactly the same (Table S3, ESI†). Generally, after binding the activator, the communications between communities around the allosteric site were increased dramatically. Community C2 and C12 in apo 15-LOX merged into one community and so did community C8 and C15. The community C9 in apo 15-LOX split into two communities, C9a and C9b. C9a is involved in formation of the active site and C9b is involved in the formation of the second AA binding site. C9b had increased motion correlations to community C7, C1, and the allosteric site (C15) which may change the variation of the second AA binding site. The communications between the N-terminal domain (C1, C13) and some communities associated with the active site (C3 and C7) were decreased. The motion correlations between communities around the active site also changed after binding the activator but not all in the same directions. In summary, the activator binding increased rigidity around the allosteric site and increased the restraint towards the second AA binding site. After the binding of the allosteric inhibitor, the number of communities decreased to 12 (Fig. 7e).

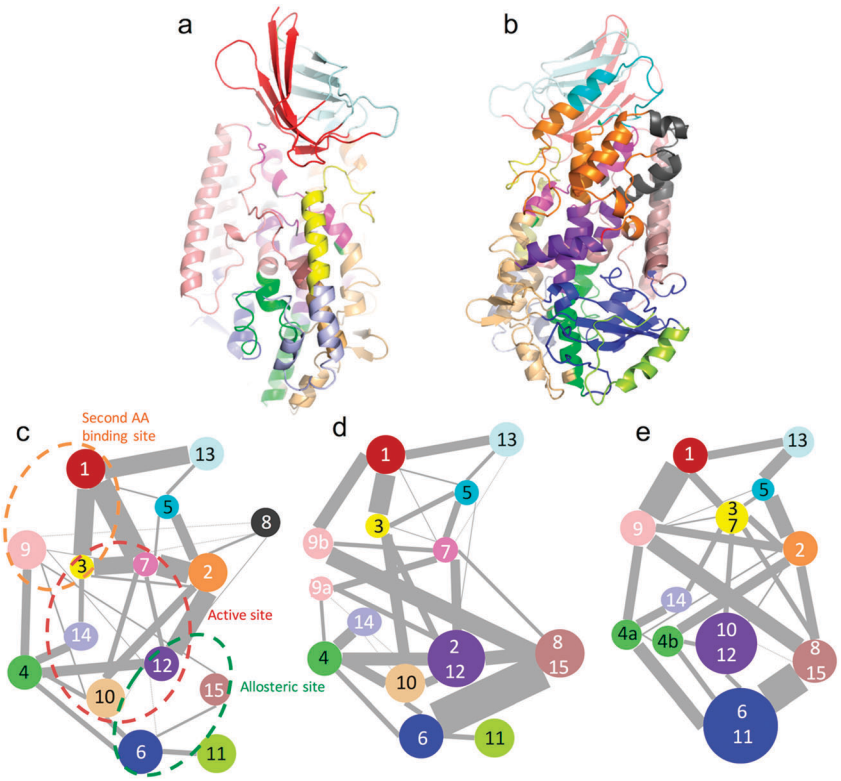

Fig. 7 Community analysis of the dynamic interactions of 15-LOX. 15-LOX carton structures (a and b) and community networks (c–e) are colored according to community membership calculated: red, 1; orange, 2; yellow, 3; green, 4; cyan, 5; blue, 6; magenta, 7; black, 8; salmon, 9; wheat, 10; lemon, 11; purple, 12; light cyan, 13; light purple, 14; brown, 15. The communities of apo 15-LOX (c), 15-LOX after the activator binding (d), and 15-LOX after the inhibitor binding (e) are presented in circles. Intercommunity connections are shown as lines, with width proportional to the cumulative betweenness of intercommunity edges.

Similar to the activator, the inhibitor increased the connection between the allosteric site and second AA binding site (community C9) as well as the connection between the N-terminal domain (community C1) and second AA binding site (community C9). Compared to the activator, the inhibitor increased the rigidity around the allosteric site and active site more significantly than the activator did. Two important communities C3 and C7 involved in composing the active site in apo 15-LOX trajectories merged into one community which may affect the function of the catalytic site. The topology of community connections around the N-terminal domain changes greatly on binding of the inhibitor which may be related to the change of relative motion in the two domains which we discovered by PCA.

Protein–ligand contacts analysis

To reveal how these two compounds affected the flexibility of the protein, we analyse the ligand-residue contacts in the MD trajectories. Using the Simulation Interaction Diagrams module in Desmond (Schrödinger, LLC), residues contacted with ligands (compounds **1** and **2**) in the last eight nanoseconds in MD simulations were recorded. The percentage of interaction time is shown in Fig. 8. We are particularly interested in hydrogen bonds and water bridges between the ligands and the protein because these interactions are generally stronger and have directional constraints, and therefore, may increase the rigidity of the system. The activator, compound **1**, contacted with D277 and R242, forming hydrogen bonds and maintaining these interactions for 100% of the simulation time, which is in agreement with the mutation experiment results (Table S4, ESI†). The inhibitor, compound **2**, contacted with V236 (back bone atom), D277 (back bone atom), and Q358 (side chain) forming hydrogen bonds and maintained these interactions for more than 80% of the simulation time. Compound **2** also contacted with R363 and A432 through water bridges for about 50% of the simulation time. Compared to the activator which had polar interactions with community C6(D277, R242) only, the inhibitor formed hydrogen bonds and water bridges with residues from three communities including C6(V236, D277), C8(Q358) and C12(A432). The formation of these H-bond networks by the inhibitor may cause the observed decrement of flexibility. Therefore, compounds that form hydrogen bonds with residues only from a single community (substructure) at this allosteric site may give a larger chance of the discovery of novel 15-LOX activators.

Discussion

The activity of 15-LOX can be allosterically inhibited by its substrate, AA, at high concentration, which was observed both in our experiment and in previous studies.[21] Experimental

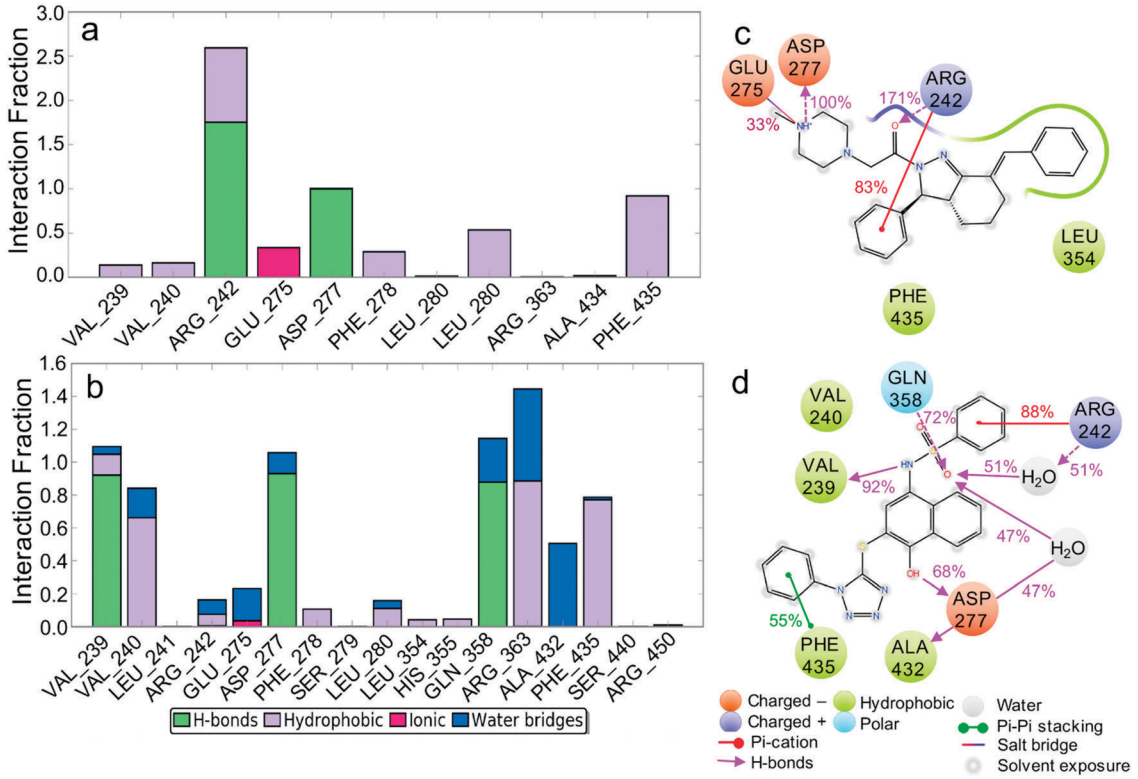

Fig. 8 Protein–ligand contacts in the MD trajectories. Protein interactions with the ligand were monitored throughout the simulation. (a) Residues contacted with compound **1**. (b) Residues contacted with compound **2**. The types of interactions were summarized, as shown in the plot above. The geometric criteria for these interactions are listed in the method section. The stacked bar charts are normalized over the course of the trajectory: a value of 0.7 suggests that for 70% of the simulation time the specific interaction is maintained. Values over 1.0 are possible as some protein residues may make multiple contacts of the same subtype with the ligand. (c) A schematic of detailed compound **1** atom interactions with the protein residues. (d) A schematic of detailed compound **2** atom interactions with the protein residues. Interactions that occur more than 30.0% of the simulation time in the selected trajectory are shown.

evidence[24,25] suggested that residues near the substrate binding site of rabbit 15-LOX contact with excessive amounts of substrate fatty acid and endogenous allosteric ligand to cause inhibition. It has also been reported that 12-LOX[21] and 5-LOX[26,27] can be regulated allosterically by AA. Interestingly, 5-LOX can be up-regulated by its substrate and some allosteric effectors[28] can inhibit 5-LOX by blocking the second, stimulating AA-binding site. Products of 5-LOX are mainly pro-inflammatory and products of 12-LOX and 15-LOX are mainly anti-inflammatory. When the concentration of AA increases, 5-LOX activity is increased while the activities of 12-LOX and 15-LOX are suppressed, which can give a fast switch of the AA network from the normal state to the inflammation state and *vice versa*. In this report, the allosteric activator, compound **1**, was found to be able to prevent this substrate inhibition and, with the increment of substrate concentration, the fold of activation increased. These findings explained the observation that compound **1** could shunt the metabolic flux towards the 15-LOX pathway in *ex vivo* assays with inflammatory stimulus[6] and also implied that this type of allosteric activator may provide a new strategy for intervention of inflammation.

In our previous work,[6] we identified a potential allosteric site of 15-LOX based on mutual information analysis. Virtual screening towards this site and experimental studies resulted in both activator and inhibitor compounds. In order to understand the allosteric activation and inhibition mechanism, in the present study, we conducted 15-LOX enzyme catalytic assays and MD simulations in the presence of the allosteric compounds. In addition to conformational analysis which helped explain the substrate inhibition mechanism of 15-LOX, we carried out further analysis on protein dynamics to understand why compounds binding at the same site resulted in opposite (activation or inhibition) effects. We found that while the activator can prevent the formation of the substrate inhibition site with no observable effect on the flexibility of the active site, the allosteric inhibitor noticeably decreases the flexibility of the active site, resulting in inhibition of 15-LOX. Community network analysis also supports these results. Compared to the activator, the inhibitor further increased the correlations between different communities around the active site of 15-LOX. Our results on 15-LOX are in accordance with recent reports[29–31] that changes in dynamics instead of conformation transitions mediate allosteric regulation. With this new knowledge that it is the change of protein flexibility that causes 15-LOX inhibition, we examined the two activators discovered by similarity screening based on compound **1**.[6] These two compounds indeed mainly interact with residues from only one community (R242 and D277) according to the molecular docking results, which is in agreement with our results in this report.

Conclusions

Using the allosteric activator and inhibitor compounds as molecular probes, we revealed the mechanism of high concentration substrate inhibition of 15-LOX and the interplay between the substrate and the allosteric compounds. Our enzyme kinetic assays and modelling studies showed that the activator compound drastically reduces the binding affinity of the second AA, thus increasing enzyme activity at a high concentration of AA. In contrast, the allosteric inhibitor decreases turnover number significantly no matter whether 15-LOX binds to the second AA or not. We found that in the MD simulations, the active site in the apo 15-LOX tends to connect to another cavity between the N-terminal and the catalytic domains, resulting a large pocket with a volume twice large as that in the starting conformation. This large pocket can well accommodate the second AA molecule and result in substrate inhibition. Binding of the activator, compound **1**, eliminates the second AA binding site, and thus activates the protein at high AA concentration. The inhibitor decreases the flexibility of the 15-LOX molecule and restrains the motions of active site residues, thus resulting in inhibition. These discoveries give guidelines for 15-LOX allosteric inhibitor and activator design: activator compounds should be able to eliminate the second AA binding while keeping the original active site dynamics; allosteric inhibitor compounds should be designed to reduce the active site dynamics.

Author contributions

H. M., Y. L., and L. L. conceived and designed the experiments. H. M. performed all the 15-LOX experimental studies, and molecular dynamics simulations of the allosteric effectors. Z. D. performed enzyme kinetics data analysis. W. Z. performed community network analysis. H. M., Y. L., and L. L. wrote the paper.

Conflicts of interest

The authors declare no competing financial interest.

Acknowledgements

We thank Dr Christopher L. McClendon for technical assistance on molecular simulation and Mr Jinxin Liu for technical support. This work was supported in part by the National Natural Science Foundation of China (21573012 and 21633001) and the Ministry of Science and Technology (2016YFA0502303 and 2015CB910300).

References

1 H. Kuhn and V. B. O'Donnell, *Prog. Lipid Res.*, 2006, **45**, 334–356.
2 C. N. Serhan, M. Hamberg and B. Samuelsson, *Proc. Natl. Acad. Sci. U. S. A.*, 1984, **81**, 5335–5339.
3 M. Leslie, *Science*, 2015, **347**, 19–21.
4 A. J. Klil-Drori and A. Ariel, *Prostaglandins Other Lipid Mediators*, 2013, **106**, 16–22.
5 J. F. Pei, N. Yin, X. M. Ma and L. H. Lai, *J. Am. Chem. Soc.*, 2014, **136**, 11556–11565.
6 H. Meng, C. L. McClendon, Z. Dai, K. Li, X. Zhang, S. He, E. Shang, Y. Liu and L. Lai, *J. Med. Chem.*, 2016, **59**, 4202–4209.
7 R. Shintoku, Y. Takigawa, K. Yamada, C. Kubota, Y. Yoshimoto, T. Takeuchi, I. Koshiishi and S. Torii, *Cancer Sci.*, 2017, **108**, 2187–2194.
8 R. Mogul and T. R. Holman, *Biochemistry*, 2001, **40**, 4391–4397.
9 Z. Dai and L. Lai, *Mol. BioSyst.*, 2014, **10**, 1385–1392.
10 M. Galassi, J. Davies, B. Gough, G. Jungman and P. Alken, *GNU Scientific Library Reference Manual*, 2011.
11 K. J. Bowers, E. Chow, H. Xu, R. O. Dror, M. P. Eastwood, B. A. Gregersen, J. L. Klepeis, I. Kolossvary, M. A. Moraes, F. D. Sacerdoti, J. K. Salmon, Y. Shan and D. E. Shaw, presented in part at the Proceedings of the ACM/IEEE Conference on Supercomputing (SC06), Tampa, Florida, November 11–17, 2006.
12 G. A. Kaminski, R. A. Friesner, J. Tirado-Rives and W. L. Jorgensen, *J. Phys. Chem. B*, 2001, **105**, 6474–6487.
13 G. J. Martyna, D. J. Tobias and M. L. Klein, *J. Chem. Phys.*, 1994, **101**, 4177–4189.
14 X. Daura, K. Gademann, B. Jaun, D. Seebach, W. F. van Gunsteren and A. E. Mark, *Angew. Chem., Int. Ed.*, 1999, **38**, 236–240.
15 Y. X. Yuan, J. F. Pei and L. H. Lai, *J. Chem. Inf. Model.*, 2011, **51**, 1083–1091.
16 Y. Yuan, J. Pei and L. Lai, *Curr. Pharm. Des.*, 2013, **19**, 2326–2333.
17 T. A. Halgren, *J. Chem. Inf. Model.*, 2009, **49**, 377–389.
18 O. Trott and A. J. Olson, *J. Comput. Chem.*, 2010, **31**, 455–461.
19 A. Sethi, J. Eargle, A. A. Black and Z. Luthey-Schulten, *Proc. Natl. Acad. Sci. U. S. A.*, 2009, **106**, 6620–6625.
20 M. Girvan and M. E. Newman, *Proc. Natl. Acad. Sci. U. S. A.*, 2002, **99**, 7821–7826.
21 J. Jankun, T. Doerks, A. M. Aleem, W. Lysiak-Szydlowska and E. Skrzypczak-Jankun, *Curr. Mol. Med.*, 2008, **8**, 768–773.
22 J. Glick, G. Santoyo and P. J. Casey, *J. Biol. Chem.*, 1996, **271**, 2949–2954.
23 C. Jacquot, A. T. Wecksler, C. M. McGinley, E. N. Segraves, T. R. Holman and W. A. van der Donk, *Biochemistry*, 2008, **47**, 7295–7303.
24 I. Ivanov, W. Shang, L. Toledo, L. Masgrau, D. I. Svergun, S. Stehling, H. Gomez, A. Di Venere, G. Mei, J. M. Lluch, E. Skrzypczak-Jankun, A. Gonzalez-Lafont and H. Kuhn, *Proteins*, 2012, **80**, 703–712.
25 R. Wiesner, H. Suzuki, M. Walther, S. Yamamoto and H. Kuhn, *Free Radical Biol. Med.*, 2003, **34**, 304–315.
26 M. Hieke, C. Greiner, M. Dittrich, F. Reisen, G. Schneider, M. Schubert-Zsilavecz and O. Werz, *J. Med. Chem.*, 2011, **54**, 4490–4507.
27 E. Bürkert, D. Szellas, O. Rådmark, D. Steinhilber and O. Werz, *J. Leukocyte Biol.*, 2003, **73**, 191–200.
28 O. Werz, D. Szellas, D. Steinhilber and O. Rådmark, *J. Biol. Chem.*, 2002, **277**, 14793–14800.
29 A. P. Kornev and S. S. Taylor, *Trends Biochem. Sci.*, 2015, **40**, 628–647.
30 J. Guo, X. Pang and H. X. Zhou, *Structure*, 2015, **23**, 237–247.
31 J. Guo and H. X. Zhou, *Biophys. J.*, 2015, **108**, 2771–2774.